Journal of Applied Polymer Science

Damage analysis of composites reinforced with Alfa fibers: Viscoelastic behavior and debonding at the fiber/matrix interface

Mokhtar Khaldi,[1,2,3] Alexandre Vivet,[2] Alain Bourmaud,[4] Zouaoui Sereir,[1] Belkacem Kada[5]

[1]LSCMI, BP 1505 EL M'Naouer, Oran, Algeria, Faculté De Génie Mécanique Université Des Sciences Et De La Technologie Mohamed Boudiaf

[2]CIMAP, F-14032 Caen; CNRS, UMR 6252, CEA, Ensicaen; Normandie Université, France

[3]Mustapha Stambouli University, Mascara, Algeria

[4]LIMATB, Université Européenne De Bretagne, France

[5]King Abdulaziz University, Jeddah, KSA

Correspondence to: M. Khaldi (E-mail: khaldimokhtar@gmail.com)

ABSTRACT: In this article, we first review state-of-the-art experimental techniques and measurements to characterize the mechanical properties of anisotropic vegetal alfa fibers, epoxy-resin, and the behavior of the interphase between the matrix and alfa fibers. Second, we conduct experimental tests to determine the mechanical properties of fibers, resin, and the interphase. Third, we carry out a series of finite element simulations to predict damage initiation and to estimate crack propagation in alfa-fiber/epoxy-resin (AFER) composites. Different tests to determine the longitudinal Young's modulus of alfa fibers and epoxy resin as well as nanoindentation tests to obtain the transverse stiffness of the fibers are presented. Experimental results from the characterization are introduced in a micromechanical model to estimate, using the concept of the energy release rate (ERR), the matrix crack, and its interaction with interfacial debonding. The wettability problems in the preparation of vegetable composites and their effect on fiber-matrix interfacial debonding are also addressed. The analysis of the damage behavior of AFER composites demonstrates that under load transverse to the fiber axis, a crack initiated in the matrix is propagated perpendicular to the direction of the load. Near the interface, the ERR decreases and this energy is higher in the presence of interfacial debonding areas generated by problems of fiber wettability. © 2016 Wiley Periodicals, Inc. J. Appl. Polym. Sci. **2016**, *133*, 43760.

KEYWORDS: composites; fibers; mechanical properties; resins; surfaces and interfaces

Received 10 November 2015; accepted 7 April 2016

DOI: 10.1002/app.43760

INTRODUCTION

Natural fibers (NF) have been successful in acquiring an increasing interest as reinforcement in composites. This is due to their outstanding properties, particularly their low density, reduced vibrations, increased acoustic behavior, ease of processing, and low production cost. Such weight-related properties make NF-reinforced composite (NFRC) lightweight materials with high specific properties.[1,2] In addition, the use of NF in composite materials, especially with thermoplastic resins, presents ecological advantages, NF-reinforced plastics using biodegradable polymer resin are the most environmentally friendly materials, since they can be composted at the end of their life cycle.[3] NFRC or bio-composites are commonly used in various fields that require lightweight, strong, and cheap reinforcements. Applications of NFRCs are found in biomedical, sport, automotive, construction, aircraft, aerospace, and maritime industries among others. It is worth noting that today NFRCs are used as renewable raw materials to develop renewable resources for a sustainable lifestyle.

However, NFRCs lack strong fiber-matrix adhesion, exhibit significant anisotropy, and show fewer mechanical properties in comparison to conventional synthetic fibers used in the reinforcement of composite materials such as carbon fibers and glass fibers. The structure and properties of NF, particularly plant fibers, are influenced by several conditions such as the region of growth, climate, age of the plant, and cellulosic content.[3–5] The hydrophilic character of NF causes toughness degradation of a NFRC that then produces a decrease in strength, a weakness in matrix-to-fiber load transfer, and early crack initiation. Hence, the integration in one framework, of advanced prediction models such as micromechanical models. Accurate numerical methods such as the Finite Element Method (FEM) and reliable tests are of prime importance to investigate and

enhance the fiber-matrix interfacial bonding, fiber reinforcing capacity, and mechanical priorities of NFRCs.

The behavior of plant fibers has been recently investigated in the literature. Baley *et al.*[6,7] studied the mechanical properties of flax fibers using micromechanical expressions, it was demonstrated that the longitudinal Young's modulus is of the order of 59 GPa and its transverse modulus is of the order of 8 GPa. Cichocki and Thomason[8] used a micromechanical semi-empirical model to estimate the anisotropy of Jute fiber. Based on their simulation results, the Jute fiber reinforced composite has a longitudinal stiffness of 39.4 GPa and a transverse Young's modulus of 5.5 GPa. Bourmaud and Baley[9] used tensile and nanoindentation tests to characterize the anisotropic behavior of hemp and sisal fiber-reinforced composites. The tests showed that the longitudinal and transversal moduli are 5.0 $\pm$1.5 GPa and 3.9 $\pm$ 0.9 GPa, respectively. Gindl *et al.*[10] used the same tests to measure the properties of cellulose. The tests revealed anisotropy of the order of 6.37. These investigations, and others, have shown that vegetal fibers have good mechanical properties and may be used as reinforcements in polymer matrices to produce low specific mass composites. Nevertheless, the high level of moisture absorption by the vegetal fibers (i.e., their poor wettability) as well as the insufficient adhesion between untreated fibers and the polymer matrix leads to debonding with age.[11]

The interfacial area between the fiber and matrix is of a prime importance in the characterization of composite materials and their performance, as it ensures the load transfer between the fibers and matrix and provides materials with a high mechanical performance. It is worth noting that many complex phenomena, such as creating links, interdiffusion, and physical interactions may arise and interact in this area.

Few studies have investigated the influence of the complex structure of the plant fibers on the adhesion properties to polymer matrices. Most of the work carried out on adhesion analysis between a plant fiber and a polymer matrix are often satisfied by the determination of an apparent interfacial shear stress and do not take in account the stiffness of the interphase.[12–18] The interphase plays a crucial role in the charge transfer and the toughness of the prepared composite.

Currently, there are several ongoing studies regarding the stiffness of Vegetable Fibers Reinforced Composites (VFRC). However, the understanding of the damage mechanisms occurring in these composites on different scales is still relatively sparse and lacks systematic development. Hence, further investigations of these mechanisms using enhanced approaches and techniques are required to reduce the present high level of uncertainty in the prediction of failure loads during the design stage.

The implementation of composite materials by processes like RTM (Resin Transfer Molding) can lead, if it is poorly managed, to a poor impregnation of the fiber preform and can generate areas of nonadhesion between the fiber and matrix.

It is now well known that the presence of defect has adverse effects on the mechanical properties of organic matrix composites. Generally, the presence of the defect is correlated with a reduction in fatigue life and an increase the sensitivity of the composite to environmental conditions.

One of the most complex micro-scale failure mechanisms of a VFRC under transverse loading is associated to the matrix and fiber-matrix interphase failure. The present work focuses on the first two steps of this failure mechanism: micro-crack initiation, and growth at the matrix-fiber interphase experiencing a defect during impregnation (wettability problems), that generates a partial debonding at the fiber-matrix interphase. The viscoelastic behavior of the matrix, coupled with the anisotropic behavior of alfa fibers is investigated.

EXPERIMENTAL

Matrix

The matrix used in this study is an epoxy resin obtained by a mixture of primary resin referenced Huntsman Araldite LY 1564, with a hardener referenced Huntsman Aradur 3487; with a weight ratio of 100/34 (For 100 g of resin 34 g of hardener is added) according to Huntsman Advanced Materials.[19] This mixture is then subjected to a total degassing process for half an hour to remove trapped air bubbles. Subsequently the mixture is cast in aluminum molds to obtain specimens of the desired dimensions and thickness. The molds filled with the mixture sequentially undergo a second degassing for a period of 1 h, a heat cycle with a firing step at 80°C for 8 h (8 h) in a holding oven, and then cooling. Through the reaction of the resin on the curing agent (polymerization) thermoset epoxy is obtained.

The behavior of the matrix is viscoelastic, as there is a functional connection between the history of stress $\sigma(t)$ and the history of deformation $\epsilon(t)$. The viscoelastic behavior is characterized in the time domain by creep and relaxation functions, J and R, respectively. These functions can be expressed, for a uniaxial behavior, by the following Boltzmann's integral equations:

$$\varepsilon(t)=\int_0^t J(t-\tau)\frac{\partial\sigma}{\partial\tau}d\tau \quad (1)$$

$$\sigma(t)=\int_0^t R(t-\tau)\frac{\partial\varepsilon}{\partial\tau}d\tau \quad (2)$$

The identification of the law associated with this type of behavior requires the implementation of several experimental tests. In addition to a monotonic tensile test, the creep, and relaxation tests demonstrate the viscous behavior of the matrix.

Alfa Fibers

Alfa fibers are extracted from the Stipa tenacissima or esparto grass plant, which grows in the North of Africa. The Esparto plant can also be found in the central and southeastern regions of Spain. It belongs to the Gramineae family and grows to a height of about 1 m.

Alfa strands were submitted to a chemical treatment with NaOH and anthraquinone. For this purpose, Alfa strands were poured into the reactor and mixed with a solution of sodium hydroxide (5%) and a solution of anthraquinone (0.1%). The fiber suspension was kept at 160 °C for 90 min with constant stirring. After this process the reaction medium was filtered and the alfa fibers were thoroughly washed with distilled water until neutralization. Finally, the alkali treated fibers were kept in the

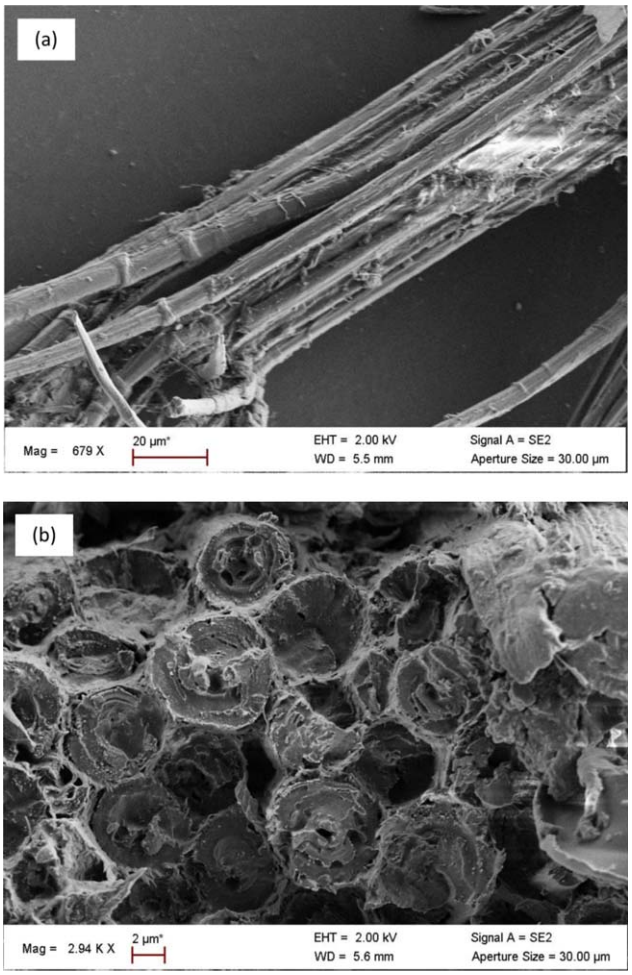

Figure 1. SEM observations of alfa fibers: longitudinal view (a) and cross-section view (b). [Color figure can be viewed in the online issue, which is available at wileyonlinelibrary.com.]

fridge at about 70% humidity in order to be used as reinforcement for the preparation of the composites.[20]

Alfa fibers have a heterogeneous structure consisting mainly of cellulose (43.9−50%), lignin (17.71−24%), hemicellulose (22.15−28%), and 5% wax.[21–25] Consequently, these fibers are highly anisotropic as are most natural fibers. Alfa fibers are circular in section with a hollow central region as shown in the SEM pictures in Figure 1(b). With a low density (1400 kg/m^3) according to NF T 20-053 Standards,[26] they are biodegradable and they come from a renewable source. Alfa fibers are actually used in the rough for handmade objects and are extracted in this state for the paper industry. Alfa plants used in this work were collected in October 2013 in the locality of Bouktob in the province of El Bayed in the west of Algeria.

Characterization of the Epoxy Resin

The characterization of the elastic and viscoelastic behavior of the epoxy resin (Araldite LY 1564/Aradur 3487) was performed at room temperature (23 ± 1 °C) using an Instron tensile machine model 8801 equipped with a capacity load cell of 5 KN. The loading curves (force-elongation) are obtained from the load cell signals (P) and an axial extensometer base of 25 mm with a maximum opening of ±5 mm is fixed on the test piece in the calibrated zone. The specimens used for the experimental tests (creep, stress relaxation, and tensile tests) are shown in Figure 2.

To define the elastic components and the fracture behavior of the matrix, tensile tests were performed on the specimens according to ISO 527-2.[27] The loading speed was 2 mm/min and the tests were carried out at least five times.

To characterize the viscoelastic behavior of the matrix, two modes of deformation were used:

- The stress relaxation test consists of imposing a deformation level on the specimen and observing the evolution of the stress versus time.
- The creep test consists of imposing a stress level and observing the evolution of the deformation as a function of time. The creep tests were performed at different levels of the average breaking stress.

Tensile Tests on Alfa Fibers

The alfa filaments were manually separated. In this work, and to simplify the analysis, each filament was considered as being perfectly cylindrical, many authors when working on plant fibers[28–30] formulate this hypothesis. An optical microscope was used to measure the apparent diameter of the filaments. The average diameter of each filament was taken at three different regions with three measurements for each region. The values of the average diameter (of ∼24–32 µm) obtained from the tested filaments and the small dimensions of single alfa fibers [Figure 1(b)] indicate that they are mainly small bundles composed of several elementary fibers.

The alfa filaments were clamped on a universal MTS Criterion tensile testing machine type 43 equipped with a 50 N capacity load cell. The filaments were loaded at a constant crosshead displacement rate of 1 mm/min up to rupture according to NT T25-503-3. The tensile tests were performed at a temperature of 23 °C and 50% relative humidity. At least 50 filaments were tested.

Nanoindentation Tests

To measure the transverse and longitudinal Young's moduli of the alfa fiber and the rigidity of the interphase, nanoindentation tests were carried out. Nanoindentation testing requires an adequate sample preparation because accurate results are obtained only if the indentations are significantly deeper than

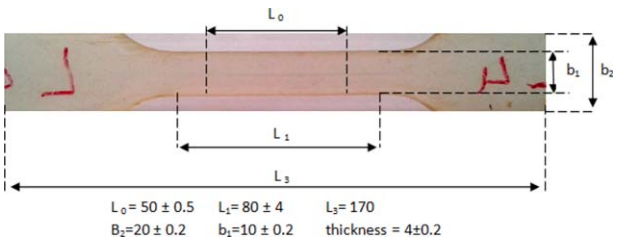

Figure 2. Geometry and dimensions of epoxy specimens according to standards ISO 727-2. [Color figure can be viewed in the online issue, which is available at wileyonlinelibrary.com.]

the surface topography of the specimen. A meticulous preparation can significantly reduce the uncertainty in determining the surface property when performing the nanoindentation test.[31] The smooth surface state is obtained with a microtome modular system equipped with a glass knife. The section is progressively cut until a nearly perfect surface state is obtained, controlled by the optical microscope. Samples are mounted on aluminum cylinders using wax for subsequent indentation tests. The nanoindentation measurements were performed using a Commercial nanoindenter (Nanoindenter XP, MTS Nano Instruments) at room temperature (23 °C) according to Li *et al.*[32] The calculation method for determining the sample module is based on the work of Oliver and Pharr.[33] Tests were carried out at a depth of between 250 and 300 nm on sections of the alfa fibers. Note that due to the very small size of single alfa fibers it is very difficult to be certain of the positioning of the indenter in the heart of the wall S2. Uncertainty exists at this level and leads to a dispersion of results. Secondly, to estimate the quality of the interphase between alfa fibers and the matrix, samples of vegetable fibers were encompassed in an epoxy resin, then two lines of 20 indents were made at the interphase between the epoxy resin and alfa fibers. The indentation depth was set at 300 nm and the gap between each indent was 1μm to avoid any overlap between the indents. In fact, the ratio of the depth and width of the footprint is about 7 for the Berkovich indenter.

Scanning Electron Microscopy (SEM)

The surfaces of the specimens were examined using a scanning electron microscope (SEM) EDAX SUPRA 55 with the following characteristics:

- Room size: $\Phi = 330$ mm and $h = 270$ mm
- Acceleration voltage: 0.1–30 kV
- Magnification: 12-900000× in SE mode and 100-900000× in AsB mode
- Focal length: 1–50 mm All

Prior to the SEM observations, a thin layer of carbon was deposited on all samples.

Modeling Technique

An energetic analysis was used to describe the matrix crack propagation process under monotonic loading. The necessary condition for the growth of a pre-existing crack in a structure is calculated according to the following relationship.

$$-\frac{deltaW_p}{deltaS} = G \geq G_c \tag{3}$$

This inequality is the Griffith criterion,[34] where $deltaW_p$ is the change in potential energy, $deltaS$ is the crack increment surface, G is the energy release rate (ERR), G_c is the fracture energy per unit surface, the so-called toughness. The ERR is perceived to be the energy required to propagate the crack per unit along the length of the crack. The objective is to compare the ERR G calculated with its critical value $G_c = G_{IC}$. The reason for the use of an ERR lies mainly in the fact that it gives an overall quantity of assumptions about the behavior of the material, so it is not restricted to linear elastic theory.

Using an asymptotic analysis, Leguillon *et al.*[35] demonstrate that near the interface the ERR of the crack can be expressed as:

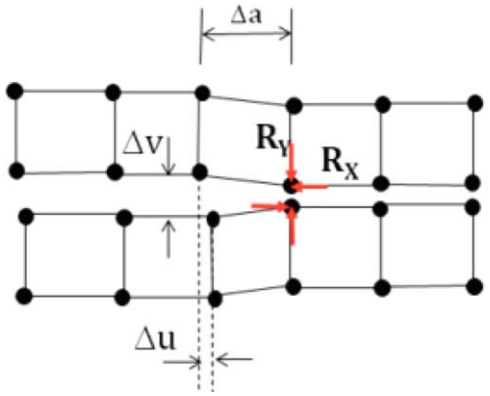

Figure 3. Parameters for VCCT for a 2D crack geometry.[38] [Color figure can be viewed in the online issue, which is available at wileyonlinelibrary.com.]

$$G(a) = K\left(\frac{a_i - a}{a_i}\right)^{2\lambda - 1}\sigma^2 \tag{4}$$

Where σ is the loading stress applied on the cracked microcomposite, K is the stress intensity factor depending only on the geometry of the specimen, while λ is the singularity coefficient. In this case the interphase is more rigid than the matrix ($E_{Interphase} > E_{Matrix}$), which defines a weak singularity with ($0.5 < \lambda < 1$), the crack is pushed back by the interface (Interphase/Matrix).

For calculating the energy release rate in ANSYS software, there are two automated methods. The first method is J-integral based method. J-integral was presented by Rice,[36] he showed the path-independence of this integral and its direct relation to energy release rate. J-integral evaluation in ANSYS is based on the domain integral method by Shih.[37]

The second automated method for calculation of the energy release rate G in ANSYS is based on virtual crack closure technique (VCCT). For automated calculation of G, ANSYS uses modified crack closure method based on VCCT and assumes that stress states around the crack tip do not change significantly when the crack grows by a small amount Δa, as shown in Figure 3. For 2D crack geometry with a low-order element mesh, the energy release rate is defined as:

$$\begin{aligned} G_I &= -\frac{1}{2\Delta a} R_Y \Delta v \\ G_{II} &= -\frac{1}{2\Delta a} R_X \Delta u \end{aligned} \tag{5}$$

where G_I and G_{II} are mode I and II energy release rates respectively, Δu and Δv are relative displacements between the top and bottom nodes of the crack face in local coordinates x and y, respectively, R_X and R_Y are reaction forces at the crack tip node, Δa is the crack extension as shown in Figure 3 taken from Ref. 38.

To simulate the evolution of the ERR of the matrix crack propagation, the modified crack closure method based on VCCT is used. As shown in Figure 4, the model is a representative volume element (RVE) consisting of a single alfa fiber with an idealized circular shape of 10 μm in diameter and an epoxy

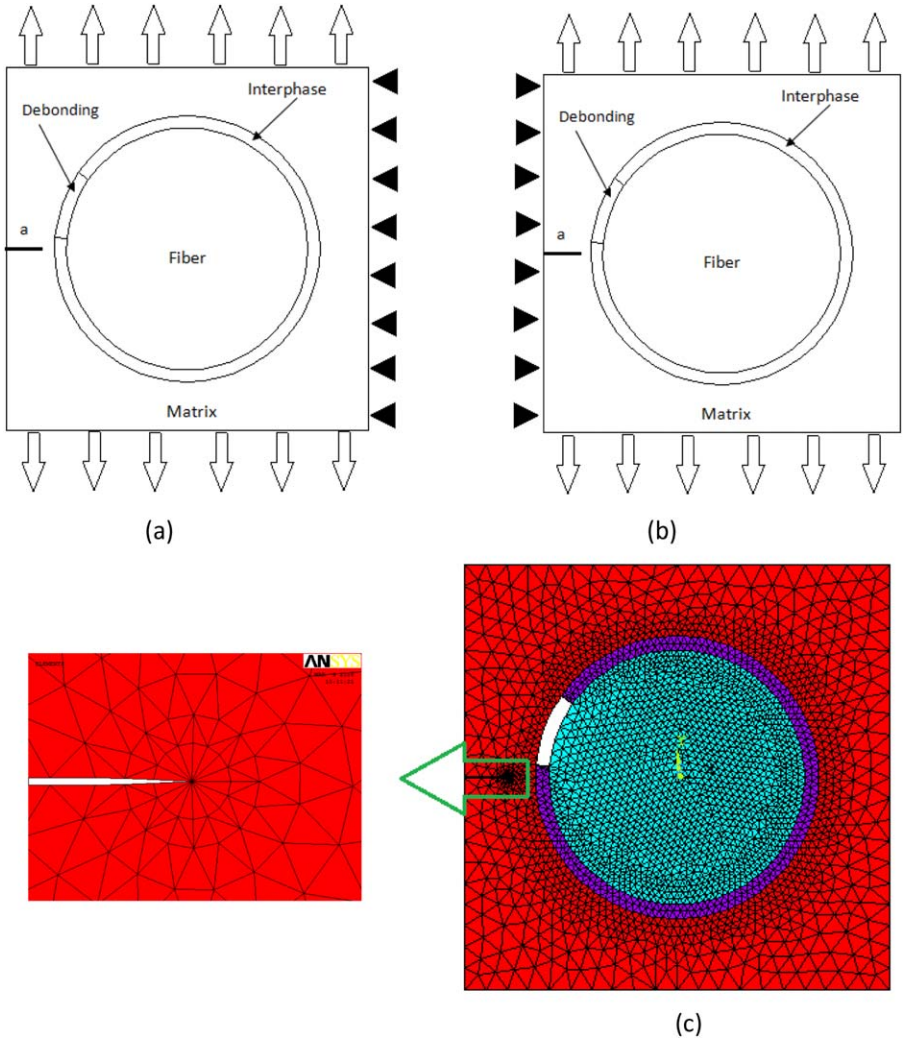

Figure 4. Model and boundary conditions used to simulate matrix crack propagation. [Color figure can be viewed in the online issue, which is available at wileyonlinelibrary.com.]

matrix. The array of the fibers is a square type. The fiber volume content is about 40%. The adhesion between the fiber and the matrix is assumed to be perfect, given the wettability problems; the debonding area is generated at the interphase between the fiber and matrix. The RVE is modeled using appropriate boundary conditions, and is subjected to a uniaxial transverse load $\sigma = 8.5$ MPa.

The fiber is meshed with 2310 ordinary isoparametric elements (PLANE 82 under ANSYS). The interphase is meshed with only 454 isoparametric elements (Plane 82). The thickness of the interphase is assumed to be 1 μm and it is also assumed to be totally cohesive, meaning that the nodal displacements at the interphase are the same regardless of the nature of the material.

The matrix is meshed using a 2D-6 node structural solid element (PLANE 183 using ANSYS software). This element is defined by 6 nodes having 2° of freedom at each node and is capable of implementing viscoelastic behavior. About 2118 elements are used to mesh the matrix. The crack tip is finely meshed with singular elements or the quarter point elements. To simulate the crack tip singularity, a particular mesh is adopted in order to have a better convergence. The element size was selected after conducting a convergence study where the ERR from the present model was compared with previous studies. Following the identification of a significant mesh size dependency, additional finite element analyses were conducted and the parametric studies were performed along the front of the crack. These results are presented and discussed in the Results and Discussion section under subsection Analysis of the Energy Release Rate.

RESULTS AND DISCUSSION

Mechanical Properties of Alfa Fibers

Figure 5 depicts the typical stress–strain curve and the evolution of the longitudinal Young's modulus of the alfa fiber. The stress–strain curve shows a nonlinear region in the early stage of the loading, this behavior may be explained by the sliding of the microfibrils along their progressive alignment with the fiber axis as reported for flax fibers.[4,39] In our case, as highlighted in the experimental section, due to the small diameter of the alfa

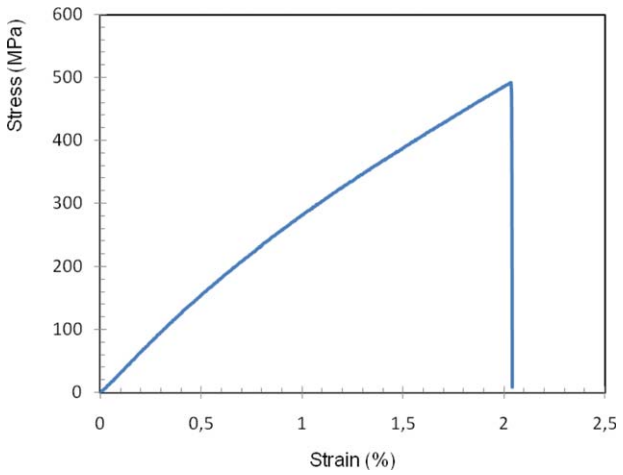

Figure 5. Typical stress–strain curve of alfa fiber. [Color figure can be viewed in the online issue, which is available at wileyonlinelibrary.com.]

fiber, around 5−8 μm [Figure 1(b)], the tested samples can be assimilated to fiber bundles and not single cells. Consequently, the tensile behavior is also dependant of the interactions within the fiber bundles. These interactions are mainly influenced by the number of fibers in the tested bundle and also by the local retting degree influencing the middle lamella quality and the cohesion between the fibers.

Table I presents the longitudinal tensile properties of alfa fibers, Poisson's ratio $v = 0.34$ is taken from the literature.[21] From these tests, an average longitudinal Young's modulus and strength at break of 28.43 ± 4.07 GPa and 474 ± 103 MPa, respectively, were obtained. As often seen on plant fibers, a moderate scattering can be observed; alfa fibers are natural products and they exhibit many defects, particularly after the fiber's extraction.

Dispersion of the properties (Young's modulus, ultimate strength, and failure strain) could also be explained by variations attributable to the area in which the fibers were taken from the plant which could be an important factor as evidenced by Charlet *et al.*[39] Furthermore, in our case, tensile tests were mainly conducted on fiber bundles and, as shown in the SEM micrograph on Figure 1(a), the diameter varies along these bundles, causing a significant discrepancy in the estimation of the average diameter and in the modulus or tensile strength results.

Using nanoindentation, the longitudinal modulus measured on the fibers alone is of the order of 20.8 ± 1.4 GPa. This result is comparable of flax modulus.[40–42] However, these results should be noted with caution because the small size of the cells can lead to an overestimation of the measurement of mechanical properties due to differences in the height of the sample near the edges of the plant cell walls. Table II shows the mean values

Table I. Longitudinal Properties of Alfa Fiber

E_L (GPa)	v	σ_r (MPa)	ε_r %
28.43 ± 4.07	0.34	474.43 ± 103.44	$2{,}43 \pm 0.58$

Table II. Values of Modules and Hardness Measured by Nanoindentation

Sample	Number of points	Young's modulus (GPa)	Hardness (MPa)
Resin	15	3.3 ± 0.2	262 ± 23
Fibers	12	20.8 ± 1.4	370 ± 54

obtained for the epoxy matrix and the fibers. These values were obtained by calculating the average values of the module and hardness between depths of 1200 to 1400 nm for the resin and between 250 and 300 nm for the alfa fibers.

Figure 6 shows the transversal Young's modulus of alfa fibers using nanoindentation with a Poisson's ratio of 0.34 for all calculations. A transversal modulus of 4.3 ± 1.4 GPa was obtained as the average value of 38 indents. Therefore, the anisotropy ratio of alfa fiber is 6.61. This ratio is comparable than the ratios of others plant fibers; Bourmaud and Baley[9] calculated an anisotropy ratio of 8.94 for hemp and 6.50 for sisal, while Baley *et al.*[6,7] have estimated the anisotropy ratio of flax fiber to be around 7.38. Table III summarizes the longitudinal rigidities and transverse modulus of our fibers and other plant fibers taken from the literature.

Mechanical Properties of the Interphase Fiber/Matrix

Figure 7 presents the evolution of the rigidity and the hardness of the interphase between alfa fibers and epoxy resin using nanoindentation. From these tests, an average Young's modulus of 17.157 ± 5.07 GPa was obtained. We observe a clear trend for the module with values close to those measured in single fibers. A slight escalation in the drop is noted at the interphase. However this must be noted with caution, edge effects or holes can disturb the measurements.

Regarding the hardness, the trend is less clear; we can see a drop followed by a rise in the interphase area which might suggest that a space may be present between the fibers and the matrix. Many authors are interested in comparing the hardness and rigidity in nanoindentation. Studies on wood walls[43–45] have shown that the modulus measured by nanoindentation was mainly influenced by the cellulose fibrils (crystallinity or cellulose rate) while the measured hardness was primarily determined by the polysaccharide matrix (hemicelluloses and

Table III. Longitudinal and Transversal Young's Modulus of Vegetable Fibers

Fiber	E_L (GPa)	E_T (GPa)	E_L/E_T	Ref.
Alfa	28.43 ± 4.07	4.3 ± 1.4	6.61	—
Flax	59	8	7.38	5
Hemp	$44{,}52 \pm 19{,}1$	$4{,}98 \pm 1{,}52$	8,94	7
Sisal	$25{,}01 \pm 12{,}9$	$3{,}85 \pm 0{,}87$	6,50	7
Jute	39,4	5,5	7,16	6
Bocell (cellulose)	$46{,}6 \pm 6{,}5$	$6{,}7 \pm 0{,}3$	7,17	8
Lyocell A (cellulose)	$31{,}2 \pm 1{,}5$	$4{,}9 \pm 0{,}2$	6,37	8

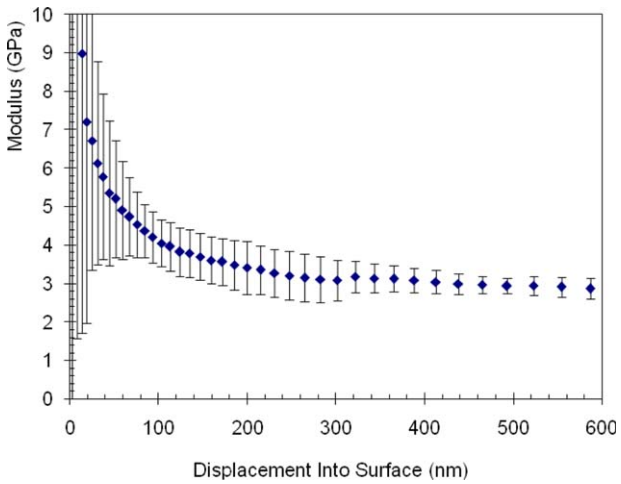

Figure 6. Results of the nanoindentation test on alfa fiber. [Color figure can be viewed in the online issue, which is available at wileyonlinelibrary.com.]

pectins). Thus, greater measured values of the fiber can be caused by a higher rate of structural polysaccharides[46] or a wall lignification.

Mechanical Properties of the Matrix

Figure 8 presents the representative conventional tensile test curves of five specimens. Table IV summarizes the results obtained. Tensile tests have confirmed the brittle behavior of the epoxy resin. A significant dispersion is observed on the strains and stresses at break. However, the difference is more consistent in terms of strain. This phenomenon is due to the presence of defects at the edges of the specimen. The measurements of elastic properties were performed on the linear portion of the curve stress/strain by linear interpolation between 0 and 1% strain. The averaged results establish the Young's modulus of the epoxy resin to be $E = 2.995 \pm 0.074$ GPa. For the fracture properties, the average values of the fracture toughness K_{1C} and the critical ERR G_{1C} of the epoxy (Araldite LY 1564/Aradur 3487) are in the range of 1 ± 0.5 MPam^2 and 280 ± 25 J/m^2, respectively.[19]

Figure 9 shows the results obtained by creep tests at different levels of the average breaking stress. From these experiments, we have drawn the evolution of the viscous deformation as a function of the creep stress by subtracting the elastic deformation from the total deformation.

Table IV. Properties of Epoxy Resin (Araldite LY 1564/Aradur 3487)

Test	E (GPa)	σ_r (MPa)	ε_r %
1	2,871	66,2	6,66
2	2,982	62,11	5,65
3	3,041	61,9	5,72
4	3,026	62,01	7,58
5	3,053	60,5	6,12
Average	2,995	62,54	6,35
Standard deviation	0,074	2,15	0,80
Manufacturer's data[19]	2.94-3.1	72-76	8.0–9.0

Figure 10 shows the characteristics of a relaxation curve. From this test, the shear and bulk moduli of the viscoelastic matrix material are defined by a Prony series expansion:

$$G(t) = G_0\left[1 - \sum_{k=1}^{n} g_k\left(1 - e^{-t/\tau_k}\right)\right] \quad (6)$$

$$K(t) = K_0\left[1 - \sum_{k=1}^{n} k_k\left(1 - e^{-t/\tau_k}\right)\right] \quad (7)$$

Where g_k, and k_k are the dimensionless shear and bulk modulus respectively and τ_k is the time relaxation material parameter. K_0 and G_0 are the instantaneous shear and bulk moduli of the linear viscoelastic material. Prony coefficients are then determined using a nonlinear regression model implemented in the ANSYS code for which a curve fitting the temporal evolutions of bulk and shear moduli are required. Table V summarizes the results obtained.

Analysis of the Energy Release Rate

The first form of damage in laminates is usually matrix microcracks. Recent works have proposed energy methods or a fracture mechanics approach to predict microcracking.[47,48] Most energy models use a finite fracture mechanics model[49,50] in which the microcrack is predicted to form when the total energy released by the formation of that microcrack reaches the

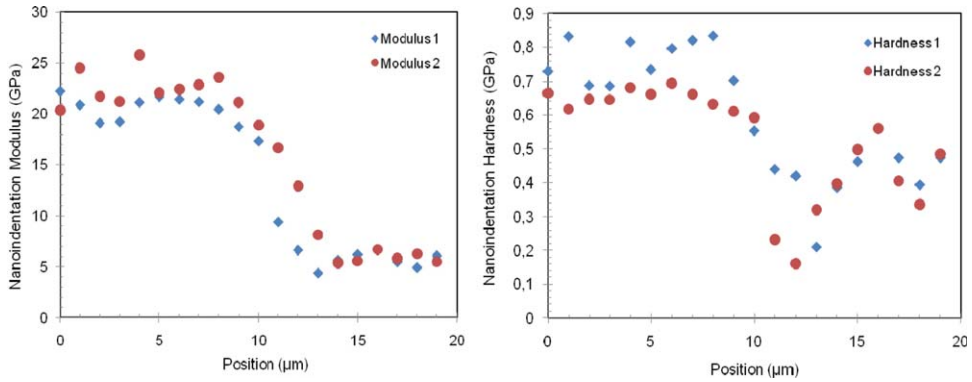

Figure 7. Evolution of the interphase (modulus and hardness). [Color figure can be viewed in the online issue, which is available at wileyonlinelibrary.com.]

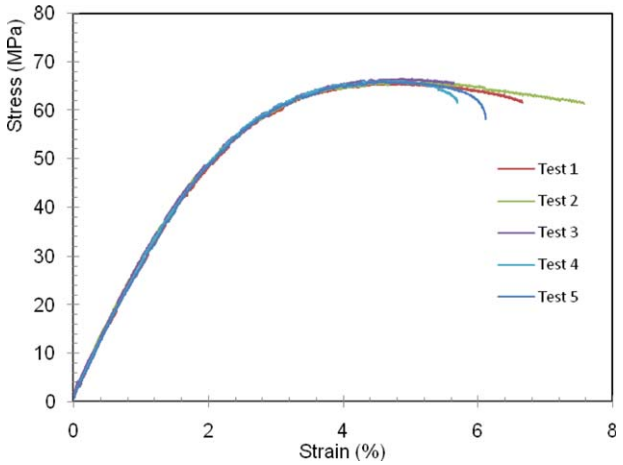

Figure 8. Tensile tests of epoxy resin (Araldite LY 1564/Aradur 3487). [Color figure can be viewed in the online issue, which is available at wileyonlinelibrary.com.]

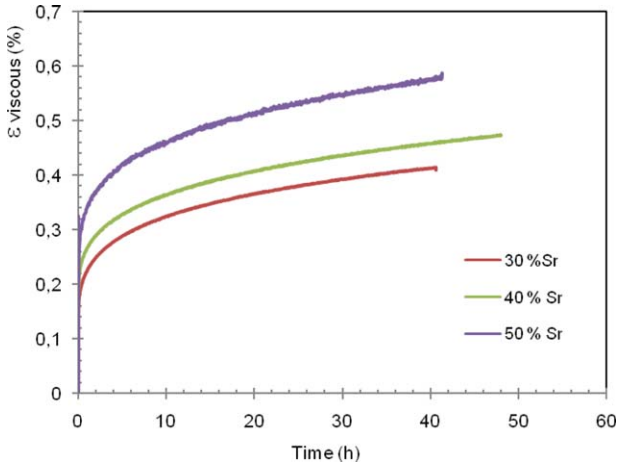

Figure 9. Creep tests of epoxy resin at different levels of breaking stress. [Color figure can be viewed in the online issue, which is available at wileyonlinelibrary.com.]

critical ERR G_c, or the microcracking toughness. Matrix microcracks are the first form of failure in many laminates.

Matrix Edge Crack. For matrix crack propagation, it is necessary for the ERR G at the crack tip to be greater than the critical ERR G_c in the range of 255–305 J/m^2.[19] In other words, $G_c = 280 \pm 35$ J/m^2 is a material property that characterizes the sensitivity of microcracking. In the case of a matrix edge crack, the results illustrated in Figure 11 show that under the action of a uniaxial load transverse to the fiber axis, a crack initiated in the matrix is propagated perpendicular to the direction of the loading, in this case the interphase and the fiber are stiffer than the matrix. Near the interphase, we observe that $G(a)$ becomes very small at the interface ($a = a_i$) and the ratio (G/G_c) of the ERR decreases. The results obtained are consistent with the asymptotic analysis of Leguillon *et al.*[35] expressed by eq. (4). In this case the interphase is more rigid than the matrix ($E_{\text{Interphase}} > E_{\text{Matrix}}$), which defines a weak singularity with ($0.5 < \lambda < 1$), the crack is pushed back by the interface (Interphase/Matrix). In the presence of a large area of non-adhesion between fiber and matrix, this rate is higher. This ratio is more than five times higher when the length of the debonding area reaches 2.61 μm, so the matrix becomes more susceptible to cracking.

Internal Matrix Crack. Figure 12 presents the evolution of the ERR for an internal matrix crack. The change in this energy is lower than in the case of edge cracks involving a slow degradation of the structure at the microscopic level. (G/G_c) decreases

Table V. Viscoelastic Property of Epoxy Resin

τ_k(s)	g_k	k_k
0.1	0.2179153	0. 6537459
1	0,37984685	1,13954055
10	0,4269061	1,2807183
100	0,37996924	1,13990772
1000	0,33096027	0,9928808
10000	0,2952962	0,8858886

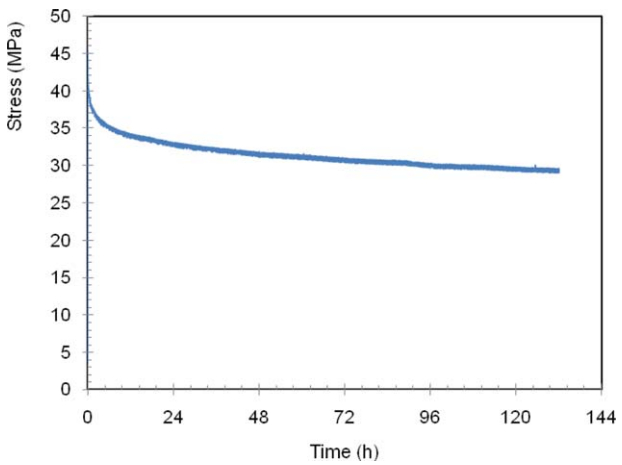

Figure 10. Epoxy resin relaxation test. [Color figure can be viewed in the online issue, which is available at wileyonlinelibrary.com.]

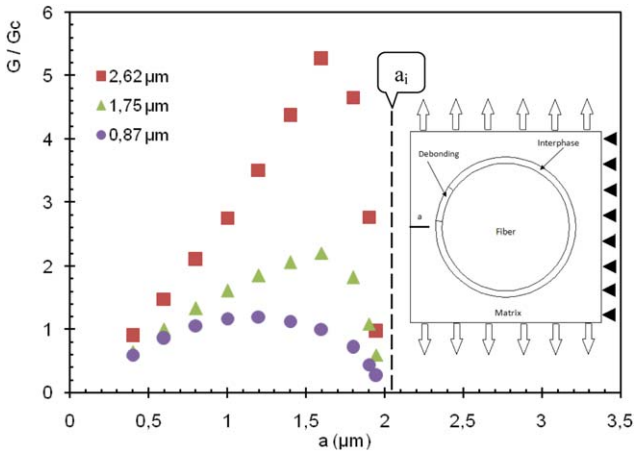

Figure 11. Evolution of the ERR of a matrix edge crack for different debonding lengths. [Color figure can be viewed in the online issue, which is available at wileyonlinelibrary.com.]

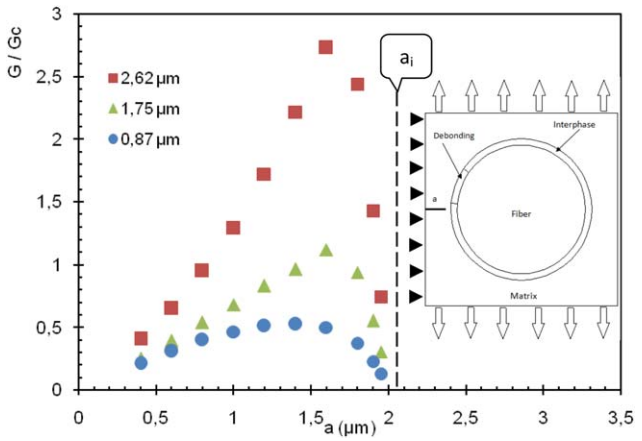

Figure 12. Evolution of the ERR of an internal matrix crack for different debonding lengths. [Color figure can be viewed in the online issue, which is available at wileyonlinelibrary.com.]

near the interface and a more stable propagation can be expected which is in good agreement with the asymptotic analysis of Leguillon *et al.*[35] expressed by eq. (4). For a debonding length that corresponds to 2.61 µm, the ERR G is about three times higher than the toughness of the matrix. For debonding lengths corresponding to 0.87 µm the maximum value of the ratio (G/G_c) is less than 1, which precludes matrix crack propagation.

CONCLUSIONS

First, a thermosetting polymer resin has been characterized by tensile tests. The transverse Young's modulus of the alfa plant fiber that can be used for the reinforcement of composites and the rigidity of the interphase were determined by nanoindentation tests. The properties of alfa fiber (longitudinal Young's modulus, ultimate strength, and failure strain) were obtained by tensile testing. The study demonstrated that nanoindentation is a suitable technique for the characterization of the transverse module of the vegetal fibers. Both characterizations have shown high anisotropy of plant fibers using experimental means. Then, the experimental results were introduced in a micromechanical model using finite element calculations to estimate the evolution of the ERR in a unidirectional composite reinforced with alfa fibers.

The developed model enabled the prediction of the effect of wettability problems on the damage behavior micromechanics of a composite with edge or internal matrix microcracks and their impact on the integrity of the structures. The growth in the size of the debonding area influences the damage behavior. On the other hand, strong interfaces can also improve crack growth resistance.

REFERENCES

1. Koronis, G.; Silva, A.; Fontul, M. *Compos. Part B: Eng.* **2013**, *44*, 120.
2. Ku, H.; Wang, H.; Pattarachaiyakoop, N.; Trada, M. *Compos. Part B: Eng.* **2011**, *42*, 856.
3. Bledzki, A. K.; Gassan, J. *Prog. Polym. Sci.* **1999**, *24*, 221.
4. Chawla, K. K.; Bastos, A. C. 3. International Conference on Mechanical Behavior of Materials; Cambridge: England, **1979**.
5. Maloney, T. M.; Lee, S. M.; Rowell, R. M. International Encyclopedia of Composites; VCH Publishers: New York, **1995**.
6. Baley, C. *Compos. Part A: Appl. Sci. Manufact.* **2002**, *33*, 939. p
7. Baley, C.; Perrot, Y.; Busnel, F.; Guezenoc, H.; Davies, P. *Mater. Lett.* **2006**, *60*, 2984. p
8. Cichocki, F. R. Jr; Thomason, J. L. *Compos. Sci. Technol.* **2002**, *62*, 669.
9. Bourmaud, A.; Baley, C. *Polym. Degrad. Stabil.* **2009**, *94*, 297.
10. Gindl, W.; Reifferscheid, M.; Adusumalli, R.-B.; Weber, H.; Röder, T.; Sixta, H., Schöberl, T. *Polymer* **2008**, *49*, 792.
11. Bledzki, A. K.; Reihmane, S.; Gassan, J. *J. Appl. Polym. Sci.* **1996**, *59*, 1329.
12. Park, J.-M.; Kim, P.-G.; Jang, J.-H.; Wang, Z.; Hwang, B.-S.; Devries, K. L. *Compos. Part B: Eng.* **2008**, *39*, 1042.
13. Towo, A.; Ansell, M.; Pastor, M.; Packham, D. *Compos. Interfaces* **2005**, *12*, 77.
14. Pommet, M.; Juntaro, J.; Heng, J.; Mantalaris, A.; Lee, A.; Wilson, K.; Kalinka, G.; Shaffer, M.; Bismarck, A. *Biomacromolecules* **2008**, *9*, 1643.
15. Czigany, T.; Morlin, B.; Mezey, Z. *Compos. Interfaces* **2007**, *14*, 869.
16. Adusumalli, R.; Weber, H.; Roeder, T.; Sixta, H.; Gindl, W. *J. Reinforced Plast. Compos.* **2010**, *29*, 2356.
17. Baley, C.; Busnel, F.; Grohens, Y.; Sire, O. *Compos. Part A: Appl. Sci. Manufact.* **2006**, *37*, 1626.
18. Le Duigou, A.; Bourmaud, A.; Davies, P.; Baley, C., "Etude des mécanismes d'adhérence entre une fibre de lin et le PLLA- Influence d'un traitement faiblement impactant à l'eau", Comptes Rendus des JNC 17 - Poitiers, **2011**.
19. Huntsman Advanced Materials. Available at: http://www.swiss-composite.ch/pdf/t-Araldite-LY1564-Aradur3486-3487-e.pdf.
20. Belhassen, R.; Boufi, S.; Vilaseca, F.; Lopez, J. P.; Mendez, J. A.; Franco, E.; Pelach, M. A.; Mutje, P. *Polym. Adv. Technol.* **2009**, *20*, 1068.
21. Brahim, S. B.; Cheikh, R. B. *Compos. Sci. Technol.* **2007**, *67*, 140.
22. Harche, M, Bounaga, D, Etude comparative du tissu fibreux dans la feuille d'alfa « Stipa tenacissima L. », Bull Soc. – Hist. Nat. Alger. **1979**, p 113.
23. Bouiri, B.; Amrani, M. *Bioresources* **2009**, *5*, 291.
24. Paiva, M. C.; Ammar, I.; Campos, A. R.; Cheikh, R. B.; Cunha, A. M. *Compos. Sci. Technol.* **2007**, *67*, 1132.
25. Ghali, L.; Zidi, M.; Roudesli, S. *J. Appl. Sci.* **2006**, *6*, 2450.
26. Standard NF T 20-053. Détermination de la masse volumique des solides en poudres et des liquides; September, **1995**.

27. ISO 527-2: Plastiques. Détermination des propriétés en traction. Partie 2: Conditions d'essai des plastiques pour moulage et extrusion, **1993**.
28. Placet, V.; Cissé, O.; Boubakar, L. *Compos. A* **2014**, *56*, 319.
29. Rosa, I. M.; Kenny, J. M.; Puglia, D.; Santulli, C.; Sarasini, F. *Compos. Sci. Technol.* **2010**, *70*, 116.
30. Alix, S.; Lebrun, L.; Marais, S.; Philippe, E.; Bourmaud, A.; Baley, C. *Carbohydr. Polym.* **2012**, *87*, 177.
31. chen, L.; Liu, T. X.; Lv, P. F. *Polym. Test.* **2005**, *24*, 746.
32. Li, X.; Bhushan, B. *Mater. Characterization* **2002**, *48*, 11.
33. Oliver, W. C.; Pharr, G. M. *J. Mater. Res.* **1992**, *7*, 1564.
34. Griffith, A. A. The Phenomenon of Rupture and Flow in Solids; Phil, Trans, Roy, Soc. London, Series A, **1920**, 221, 163.
35. Leguillon, D.; Sanchez-Palemcia, E. Fracture in Heterogeneous Materials-Weak and Strong Singularities; New Advances in Computational Structural Mechanics. Studies in Applied Math, 32, Elsevier: Amsterdam. **1992**, p 423.
36. Rice, J. R. *J. Appl. Mech.* **1968**, *35*, 379.
37. Shih, C. F.; Moran, B.; Nakamura, T. *Int. J. Fracture* **1986**, *30*, 79.
38. ANSYS. User manual, version 13. Canonsburg, PA, USA.
39. Charlet, K.; Baley, C.; Morvan, C.; Jernot, J. P.; Gomina, M.; Breard, J. *Compos. Part A: Appl. Sci. Manufact.* **2007**, *38*, 1912.
40. Bourmaud, A.; Baley, C. *Polym. Degrad. Stabil.* **2010**, *95*, 1488.
41. Bourmaud, A.; Baley, C. *Compos. Part B: Eng.* **2012**, *43*, 2861.
42. Marrot, L.; Lefeuvre, A.; Pontoire, B.; Bourmaud, A.; Baley, C. *Ind. Crops Prod.* **2013**, *51*, 317.
43. Eder, M.; Arnould, O.; Dunlop, J. W. C.; Hornatowska, J.; Salmén, L. *Wood Sci. Technol.* **2013**, *47*, p. 163.
44. Gindl, W.; Gupta, H. S.; Schöberl, T.; Lichtenegger, H. C.; Fratzl, P. *Appl. Phys. A: Mater. Sci. Proc.* **2004**, *79*, 2069.
45. Hosseinaei, O.; Wang, S.; Rials, T. G.; Xing, C.; Zhang, Y. *Cellulose* **2011**, *18*, 841.
46. Konnerth, J.; Gierlinger, N.; Keckes, J.; Gindl, W. *J. Mater. Sci.* **2009**, *44*, 4399.
47. Tan, S. C.; Nuismer, R. J. *J. Comp. Mater.* **1989**, *23*, 1029.
48. Varna, J.; Berglund, L. A. *J. Reinf. Plast. Comp.* **1992**, *11*, 708.
49. Hashin, Z. *J. Mech. Phys. Solids* **1996**, *44*, 1129.
50. Nairn, J. A. Applications of Finite Fracture Mechanics for Predicting Fracture Events in composites; Fifth Int. Conf. on Deformation and Fracture of Composites **1999**, p 1.

SGML and CITI Use Only
DO NOT PRINT